nature geoscience

Article

https://doi.org/10.1038/s41561-025-01683-7

A seawater oxygen oscillation recorded by iron formations prior to the Great Oxidation Event

Received: 3 July 2024

Accepted: 24 March 2025

Xueqi Liang[1]✉, **Eva E. Stüeken**[2], **Daniel S. Alessi**[1], **Kurt O. Konhauser**[1,3] & **Long Li**[1]

Earth's atmosphere underwent permanent oxidation during the Great Oxidation Event approximately 2.45–2.22 billion years ago (Ga) due to excess oxygen (O_2) generated by marine cyanobacteria. However, understanding the timing and tempo of seawater oxygenation before the Great Oxidation Event has been hindered by the absence of sensitive tracers. Nitrogen (N) isotopes can be an indicator of marine oxygenation. Here we present an ~200 Myr nitrogen isotope oscillation recorded by Neoarchaean and Palaeoproterozoic banded iron formations from the Hamersley Basin, Western Australia, that were deposited in relatively deep marine shelf environments. Paired with the Jeerinah Formation shale record, our data from the Marra Mamba Iron Formation suggest that oxic conditions expanded to banded iron formation depositional environments from ~2.63 to 2.60 Ga. Subsequently, a positive $\delta^{15}N$ excursion occurred in the ~2.48 Ga Dale Gorge Member, marking a decline in seawater O_2 and enhanced denitrification. This O_2 deficit was followed by a second phase of increasing O_2 levels as indicated by a gradual return to moderately positive $\delta^{15}N$ values in the ~2.46 Ga Joffre Member and 2.45 Ga Weeli Wolli Iron Formation. These variations underscore a nonlinear history of marine oxygenation and reveal a previously unrecognized oscillation in seawater O_2 levels preceding the Great Oxidation Event.

The prevailing narrative attributes the Great Oxidation Event (GOE) to a progressive accumulation of O_2 in shallow marine 'oxygen oases', which subsequently released O_2 into the atmosphere, eventually surpassing the flux of atmospheric reductants[1]. Understanding when and how seawater became oxygenated is crucial for comprehending the overall oxygenation of the atmosphere, but this timeline remains poorly constrained. Numerous attempts to estimate the timing of seawater oxygenation have yielded a range that spans over a billion years. For example, previous studies proposed that oxygenation of the ocean's surface was recorded in the 2.5 billion years ago (Ga) Mount McRae Shale on the basis of redox-sensitive elements such as uranium (U), molybdenum (Mo) and sulfur (S), along with Mo and thallium (Tl) isotope fractionation[2,3]. Similarly, in the 2.7–2.6 Ga black shales from Western Australia, South Africa and Zimbabwe, indices such as Mo, rhenium (Re) and osmium (Os) enrichments, as well as iron (Fe) speciation and isotope fractionations of Fe, Mo, S and carbon (C) isotopes, collectively point to the existence of O_2-rich environments at that time[4]. However, in apparent contrast, a survey of seven banded iron formations (BIFs) from 2.6 to 2.5 Ga across the North China Craton used multiple geochemical indices, such as cerium (Ce) anomalies, positive Fe isotopes and the lack

---

[1]Department of Earth and Atmospheric Sciences, University of Alberta, Edmonton, Alberta, Canada. [2]School of Earth and Environmental Sciences, University of St Andrews, St Andrews, UK. [3]Department of Earth and Environmental Sciences, University of Manchester, Manchester, UK.
✉e-mail: xueqi5@ualberta.ca

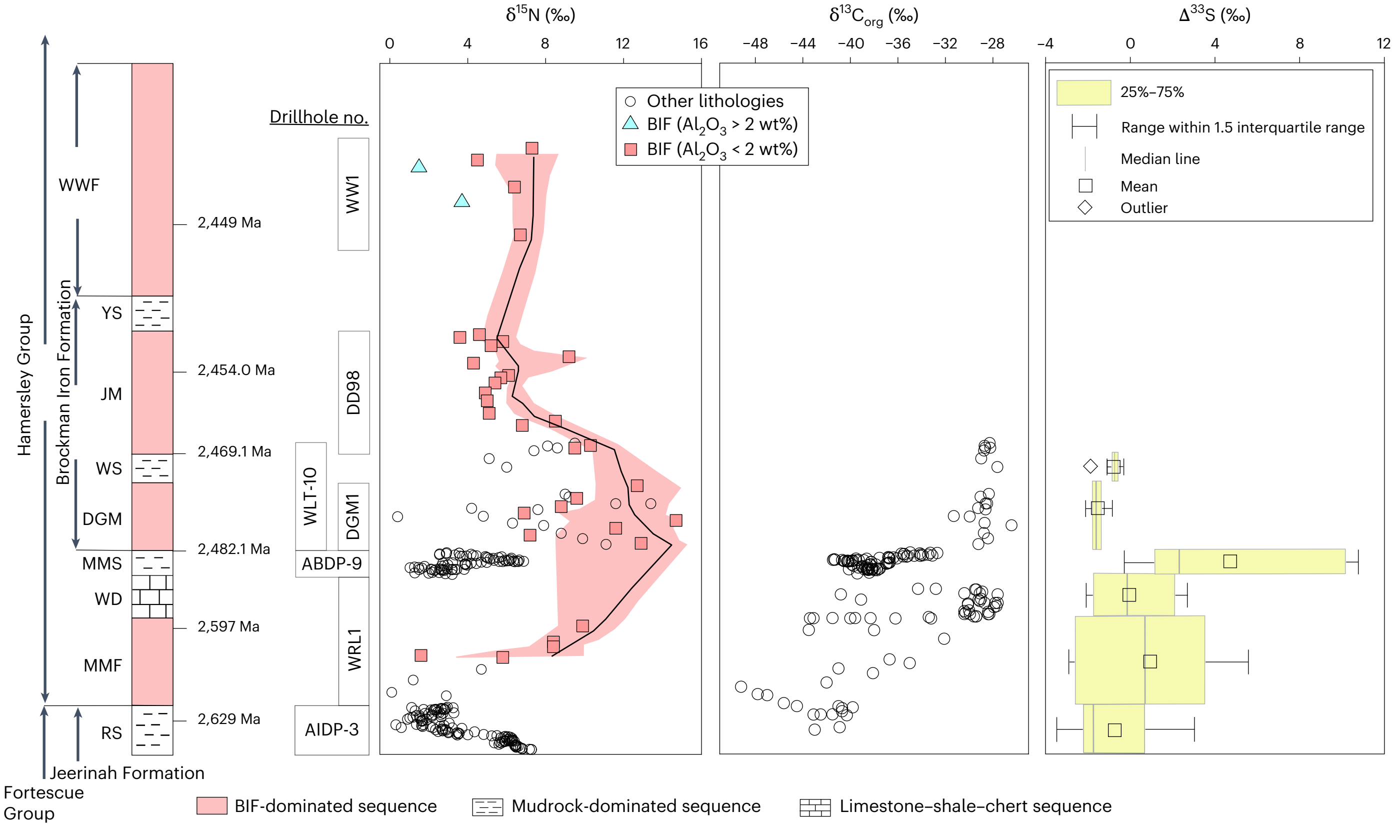

Fig. 1 | Simplified stratigraphy and isotopic profiles of sediments in the Hamersley Group. The 2σ error bars of the data are smaller than the symbols and thus not shown. BIF $\delta^{15}N$ data were fitted using the LOWESS model, with the 1σ confidence interval band shown as a shaded area. For comparison, the $\delta^{15}N$ values[2,21,22,26], $\delta^{13}C_{org}$ values[2,22,48] and $\Delta^{33}S$ values (presented as a box plot)[43,49] of the interlayered units are also included. Data points are positioned on the stratigraphic column on the basis of the depth data of each sediment unit and each sample in the drill cores. Detailed age constraints are discussed in Methods. WWF, Weeli Wolli Formation; YS, Yandicoogina Shale; JM, Joffre Member; WS, Whaleback Shale; DGM, Dales Gorge Member; MMS, Mt McRae Shale; WD, Wittenoom Formation; MMF, Marra Mamba Formation; RS, Roy Hill Shale Member.

of enrichments in manganese (Mn), chromium (Cr) and arsenic (As), to demonstrate low O_2 in the water column[5]. Reference 6 suggested that an increase in the total S and Mo supply to marginal marine sediments at 2.8 Ga was best explained by biological oxidation of sulfide minerals in the crust. In addition, U enrichment and the isotopic patterns of Mo, Cr and S in the ~2.95–2.97 Ga BIFs and dolomites from South Africa were interpreted as evidence of partial oxygenation of surface environments[7]. Reference 8 suggested the existence of oxygenic photosynthesis and oxygenated seawater on the basis of C isotopic signatures and elevated U/thorium (Th) ratios in the >3.7 Ga metamorphosed pelagic shales in West Greenland. However, distinguishing between in situ marine production and terrestrial input using these geochemical indices can be challenging. For example, elemental enrichments in Mo, U and S are commonly linked to oxidative weathering on land, where O_2 could be derived from sources that include whiffs of O_2 from marine oxygen oases[9], terrestrial benthic cyanobacterial mats on land[10] or abiotic production through water–mineral reactions[11].

Nitrogen as a crucial proxy for seawater redox conditions

Nitrogen (N) plays a dual role as a crucial trace element in seawater and a fundamental constituent of life, owing to its diverse stable redox states. The isotopic signatures of these N forms are results of various N isotope-discriminating processes in aqueous environments. This makes N isotopes a valuable indicator of marine oxygenation[12], which has profoundly regulated the evolution of the global biogeochemical N cycle[13]. Before the emergence of oxygenic photosynthesis, the N cycle probably involved predominantly reduced species. Nitrogen-fixing organisms utilize atmospheric dinitrogen (N_2) to synthesize organic matter, with minor isotope fractionation. Despite experimental results[14] showing that the N isotope enrichment factor ($\varepsilon \approx \delta^{15}N_{product} - \delta^{15}N_{reactant}$) of this process can vary from −8‰ to +1‰, the $\delta^{15}N$ values of diazotrophic biomass mostly fall in the range of −4‰ to 0‰ (ref. 15). In oxygenated oceans, nitrification generates abundant nitrate (NO_3^-) and/or nitrite (NO_2^-). Although the ε values typically range from −25‰ to −1‰, they are rarely expressed in biomass because nitrification rapidly goes to completion at sub-micromolar O_2 levels[13,16]. Similarly, the isotope fractionation associated with NO_3^- assimilation (−10‰ to −5‰) is often not observed because this process typically goes to completion[17]. In suboxic settings, denitrification (ε up to −30‰)[16,18] and/or anaerobic ammonium oxidation (anammox; ε up to −26‰) releases ^{15}N-depleted N_2 gas, which can progressively increase the $\delta^{15}N$ value of the residual NO_3^-. A similar fractionation occurs during dissimilatory nitrate reduction to ammonium[19], but this metabolism has not yet been systematically studied.

On the basis of N isotopic data of marine sediments, several studies have proposed that the surface oceans experienced oxygenation during the Neoarchaean and Palaeoproterozoic eras. For example, ref. 20 reported a $\delta^{15}N$ increase in kerogen from 0‰ to ~+2‰ at 2.67 Ga in the Campbellrand Group in South Africa. This shift was interpreted as evidence for the onset of coupled nitrification and denitrification, or anammox, in the surface oceans[20]. In the 2.66 Ga Jeerinah Formation in the Hamersley Basin in Western Australia, shales recorded $\delta^{15}N$ fluctuations between +2‰ and +6‰, suggesting a period of transient surface ocean oxygenation lasting ~50 Myr (ref. 21). Similarly, ref. 2 observed a $\delta^{15}N$ variation from +1.0‰ to +7.5‰ in the 2.5 Ga Mount McRae Shale in Western Australia, concurrent with a rise in atmospheric

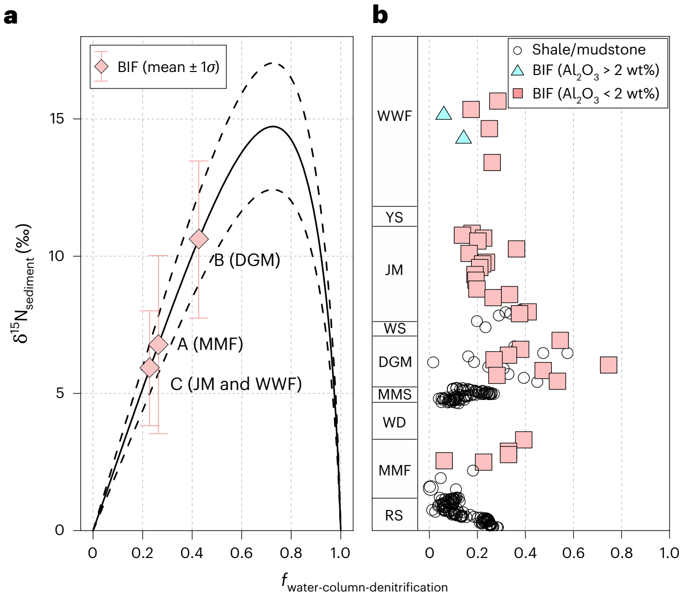

Fig. 2 | Modelling the degree of denitrification for sedimentary rocks in the Hamersley Basin. a, Modelling (Methods) the change of sedimentary $\delta^{15}N$ values along progressive water-column denitrification in a closed system using isotope fractionation factors of −26 ± 4‰ (dashed curve and shaded area). Embedding the average $\delta^{15}N$ values of the Marra Mamba, Dales Gorge and Joffre + Weeli Wolli BIFs on the curve indicates that (1) anoxia expanded in the surface water from the Marra Mamba Iron Formation to the Dales Gorge Member, leading to an increase in the degree of denitrification (point A to point B); (2) from the Dales Gorge Member to the Weeli Wolli Iron Formation, O_2 became more pervasive in surface water, resulting in a decrease in the degree of denitrification (point B to point C). **b**, Calculated degrees of water-column denitrification for individual samples from the sediment units in the Hamersley Basin. Data source and symbols are the same as in Fig. 1.

O_2 as indicated by Mo enrichments. Those authors proposed a transient occurrence of coupled nitrification–denitrification due to increased nutrient input from oxidative weathering on land. In addition, several studies[22–25] have reported positive $\delta^{15}N$ values between +2‰ and +8‰, with occasional values up to +12‰ in the early Palaeoproterozoic. This indicates the establishment of a moderately stable NO_3^- reservoir in the surface ocean at that time, albeit punctuated by periods of NO_3^- depletion. Collectively, the existing data suggest that seawater O_2 appeared transiently as early as 2.67 Ga.

However, previous N isotopic studies have relied primarily on discrete shales and mudstones[2,21,22,26], with each formation/member recording a temporal scale of less than 50 Myr (refs. 9,21,27,28) (see 'Age constrains' in Methods). This leaves notable time gaps in the N isotopic record and makes it difficult to determine the timescales over which oxic conditions waxed and waned and whether these fluctuations align with reported sulfur mass independent fractionations (for example, ref. 29). BIFs, another type of environmental record, are more continuously deposited over longer periods at the Archaean/Proterozoic boundary, but their N isotope signatures remain underexplored. Furthermore, unlike shales, which were deposited in shallower-water environments and could be influenced by detrital minerals from oxidative weathering on land and/or terrestrial nitrate run-off[30], BIFs offer insights into deeper marine shelf environments (for example, ref. 31). Exploring N isotopes in the BIF record may help to further advance our understanding of early marine oxygenation.

N isotopic signatures of Hamersley BIFs

BIFs are important sedimentary archives spanning the GOE that are well represented in the Hamersley Basin. BIFs are characterized by scarce organic matter but abundant authigenic/diagenetic minerals[32,33]. This scarcity of organic matter, such as planktonic biomass, may be attributed to processes such as dissimilatory iron reduction, which can efficiently degrade biomass to bicarbonate (HCO_3^-) and ammonium (NH_4^+) ions[34]; the latter can then enter potassium (K)-bearing diagenetic minerals in BIFs through substitution[12]. For our N isotope study, we selected well-characterized BIFs spanning ~2.60–2.45 Ga in the Hamersley Group, Pilbara region of Western Australia (Extended Data Figs. 1–3 and Supplementary Information). By integrating these data with previous findings from the underlying and interbedded carbonate and shale layers—specifically the Jeerinah Formation and the Mt McRae shales—we provide an ~200 Myr N isotopic record leading up to the GOE.

In the Hamersley Group BIF column (Fig. 1a and Extended Data Table 1), $\delta^{15}N$ values show a steady increasing trend from ~+2‰ to ~+10‰ over the 2.60 Ga Marra Mamba BIF. The $\delta^{15}N$ values reach a peak at ~+15‰ in the 2.48 Ga Dales Gorge Member BIF, followed by a gradual decrease to ~+4‰ to +7‰ in the 2.46 Ga Joffre BIF. This low $\delta^{15}N$ range persists through the 2.45 Ga Weeli Wolli BIF.

Environmental implications

The total nitrogen contents of the BIF samples exhibit a positive relationship with their K contents ($R^2 = 0.66$; Extended Data Fig. 4). This correlation verifies that N in the BIF samples is present primarily as NH_4^+ substituting for K^+ in silicate minerals (mainly stilpnomelane with small amounts of K-feldspar and ferri-annite; Supplementary Information). Since the incorporation of aqueous NH_4^+ into phyllosilicate minerals results in little N isotope discrimination[35], the $\delta^{15}N$ values of these silicate minerals can effectively represent the isotopic signature of dissolved NH_4^+ in the diagenetic fluid from which these minerals precipitated.

Considering the low metamorphic grades of the studied Hamersley BIF samples (prehnite–pumpellyite facies for drill cores WRL1, DGM1 and DD98, and greenschist facies for the Weeli Wolli BIF in drill core WW1), the $\delta^{15}N$ values of the BIFs should have been minimally affected by metamorphic N devolatilization, which occurs mostly at higher temperatures[36]. This is further verified by the discrepancies between our data and the expected metamorphic N devolatilization trend (Extended Data Fig. 5). Therefore, the $\delta^{15}N$ values of the studied BIFs are considered to closely reflect their original N isotopic signature, within a margin of 1–2‰, making them a robust tool for inferring the seawater N cycle.

The $\delta^{15}N$ values up to +7‰ from the underlying ~2.63 Ga Jeerinah Formation shales have previously been interpreted as evidence of aerobic N cycling paired with partial denitrification along a redoxcline in the water column[21]. Interestingly, comparably low $\delta^{15}N$ values extend into the lower section of the Marra Mamba BIF, suggesting that a similar N cycle persisted in the deeper depositional environment of BIF until ~2.60 Ga. Sedimentary denitrification does not impart a large net isotopic effect ($\varepsilon < -3$‰) and is ~80 times slower than water-column denitrification[24]. The degree of water-column denitrification (Fig. 2; see 'Box model' in Methods and Extended Data Fig. 6) cannot be unambiguously determined from the data; however, the extremely low $\delta^{13}C_{org}$ values from the interbedded mudstones in the lower Marra Mamba BIF suggest an appreciable role for methanotrophs in the concurrent marine C cycle. These microbes were capable of aerobic or anaerobic oxidation of methane (CH_4), utilizing either O_2 or other electron acceptors, such as sulfate (SO_4^{2-}), NO_3^-, Fe(III) oxyhydroxides or Mn(IV) oxides[37–40]. Aside from Fe(III) oxyhydroxides, these electron acceptors are all indirectly related to O_2 since NO_3^-, SO_4^{2-} and Mn(IV) are derived mainly from the oxidation of NH_4^+, HS^- and Mn(II) by O_2, respectively[41]. Hence, we posit that the lower Marra Mamba BIF was deposited in an oceanic setting with O_2 oases in shallow waters to support aerobic metabolic pathways (Fig. 3a). The degree of water-column denitrification was probably relatively small in this basin (~10–30%;

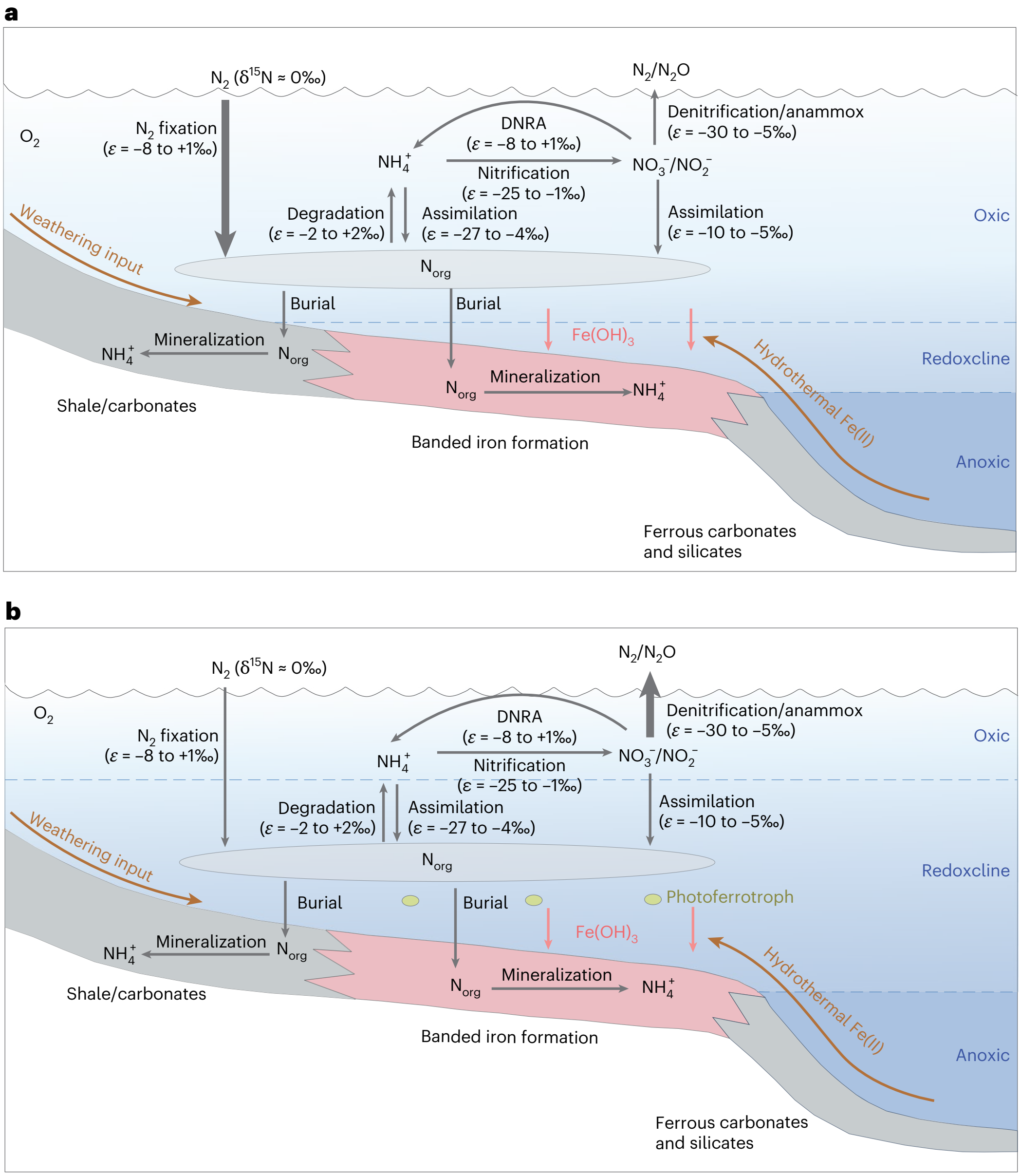

Fig. 3 | Depositional models (not to scale) for Hamersley BIFs. The cartoon illustrates predominant processes in the biogeochemical N cycle under different redox conditions. The relative thickness of the N pathway (lines with arrows) marks the relative magnitude of N along that pathway. **a**, The scenario produces moderate δ^{15}N values in BIFs. **b**, The scenario gives high δ^{15}N values (see text for detailed explanation). DNRA, dissimilatory nitrate reduction to ammonium.

Fig. 2), similar to today, implying that NO_3^- was able to accumulate down to the sediment–water interface.

The increasing δ^{15}N trend towards the upper Marra Mamba BIF and into the Dales Gorge Member can be best attributed to enhanced water-column denitrification (up to ~70%; Fig. 2). This would suggest a decline in the size of the NO_3^- reservoir, probably linked to decreasing availability of O_2, a more energetically favourable terminal electron acceptor. This implies that the O_2 oasis recorded by the Jeerinah Formation probably receded over time, with NO_3^- replacing O_2 as the major electron acceptor. Although the Feammox reaction (anaerobic oxidation of NH_4^+ to N_2 by ferric oxyhydroxides) could increase the δ^{15}N value of remaining NH_4^+ (ref. 42), it is not the preferred explanation for our data because Feammox requires a completely anoxic environment[22], which is inconsistent with the observed aerobic N cycle in the underlying Jeerinah Formation shales and the lower Marra Mamba BIF. Furthermore, Feammox would not explain the secular trend observed in BIFs in the Hamersley Group.

The δ^{15}N peak of ~+15‰ in the Dales Gorge BIF thus indicates a sustained period of O_2 deficiency (Fig. 3b), over which the NO_3^- reservoir became more limited and the isotopic effect from water-column denitrification became more prominent (up to ~70%). The δ^{15}N peak lingered over the Dales Gorge BIF while their interbedded mudstones show suppressed Δ^{33}S values[43] around 0‰ and elevated $\delta^{13}C_{org}$ values around −28‰ (ref. 22), which indicate the sustained presence of at least some atmospheric O_2 (ref. 43). The concurrent offshore decline in the NO_3^- reservoir may be a result of its enhanced utilization at that time.

The δ^{15}N values of BIF display a steady decrease in the lower Joffre BIF and are stabilized in the range of +4‰ to +7‰ throughout the upper Joffre and the Weeli Wolli BIFs (Fig. 1). We first examined whether this decreasing trend was attributed to a gradual shallowing of the BIF depositional environment, given the observation that shales and mudstone deposited in shallower water have on average lower δ^{15}N values than coeval BIFs (Fig. 1), possibly due to higher contents of diazotrophic biomass (N_2-fixing bacteria; δ^{15}N = ~0‰) and/or detrital minerals in shallow sediments (more discussion follows). Consequently, relative sea-level decrease would move the redoxcline more proximal and thus decrease the $\delta^{15}N$ values of BIFs. However, this is unlikely to apply to our samples as the relative sea-level changes among the depositional environments of BIFs are negligible compared with the much shallower depositional environments of the shale units[31]. In addition, aluminium (Al) is a common element in continental N-bearing minerals[44] and can be used as an index of detrital minerals in BIFs. Several observations on the Al_2O_3 contents (Extended Data Fig. 7) indicate that N in the BIFs is not associated with detrital minerals, including (1) all samples (except two in the Weeli Wolli BIFs) contain relatively low Al_2O_3 contents (0.09–1.44 wt%; average: 0.43 wt%); (2) the two exceptional Weeli Wolli samples with relatively high Al_2O_3 contents (>2 wt%) contain very low N contents (<20 $\mu g\ g^{-1}$); (3) the BIF samples with high N contents (>40 $\mu g\ g^{-1}$) all have low Al_2O_3 contents around 0.5 wt%; and (4) no positive relationship ($R^2 = 0.02$) is observed between total N contents and Al_2O_3 contents.

Accordingly, the $\delta^{15}N$ decrease in the lower Joffre Member and levelling off throughout the upper Joffre and the Weeli Wolli BIFs indicate a progressively diminishing role of water-column denitrification, implying the regrowth of the NO_3^- reservoir (Fig. 2). This interpretation is consistent with concurrent $\Delta^{33}S$ suppression[43], the elevated $\delta^{13}C_{org}$ (ref. 22) and oxidative continental weathering-induced Cr enrichment in the Weeli Wolli BIFs[45]. Collectively, these data point to an increase in seawater O_2 levels.

Interestingly, there exists a small $\delta^{15}N$ peak of ~+9.2‰ in the upper Joffre (DD98-7)—albeit just one data point—that might suggest that O_2 levels could have temporarily decreased during this overall increasing oxygenation trend. Relatively low $\delta^{15}N$ values (<8‰) are also observed in the $\delta^{15}N$ peak period in the Dale Gorge BIFs, which might suggest transient seawater O_2 increase in this overall O_2 deficit period. Short-term (for example, precession-scale) redox variations have been reported from the 2.46 Ga Joffre BIFs[46]. These are worth further studies on N isotopes when high-resolution samples are available.

Complementary $\delta^{15}N$ signals in BIFs and shales

The $\delta^{15}N$ signals of BIFs and shales in the Hamersley Basin exhibit overlap during certain periods (for example, the Jeerinah–Marra Mamba transition; Fig. 1) but diverge at other times. This variability is expected and does not conflict with our interpretation given the different depositional environments of these sediments, which record the N isotopic signatures of different N contributors. For example, the underlying and interbedded shales, enriched in organic matter with over 10 wt% total organic carbon in some locations[2,21], suggest a high level of productivity. This productivity could have been supported by a substantial NO_3^- reservoir in shallow waters, which could exist if water-column denitrification rates were relatively low, as suggested by our model calculations (see 'Box model' in Methods). In addition, diazotrophic biomass might have evidently contributed to the high total organic carbon contents in shales. Biomass derived from either diazotrophic processes or low levels of denitrification typically have relatively lower $\delta^{15}N$ values. By contrast, BIFs capture the $\delta^{15}N$ signature of the offshore NO_3^- reservoir, located closer to the anoxic deep ocean (Fig. 3). When $\delta^{15}N$ values in BIFs are higher than those in shales, it suggests a relatively greater degree of water-column denitrification in offshore regions. The long-term $\delta^{15}N$ trends in the BIF record therefore reflect the waxing and waning in the offshore NO_3^- reservoir. The onshore NO_3^- reservoir probably experienced similar oscillations over time, possibly in synchrony with offshore changes. While BIFs and shales represent distinct depositional settings and record different $\delta^{15}N$ signatures, their complementary perspectives provide a more comprehensive understanding of the marine N cycle and its relationship to ocean oxygenation over time.

Seawater N cycle in the Hamersley Group

In summary, the N isotope record in the Hamersley Basin reveals an ~200-Myr-long oscillation in seawater O_2 levels and NO_3^- availability leading up to the GOE[47]. The ~2.48 Ga Dales Gorge Member records retrograding seawater O_2, conducive to enhanced denitrification in the water column, following earlier oxygenation events recorded in the ~2.63 Ga Jeerinah Formation and ~2.60 Ga Marra Mamba Iron Formation. Afterwards, O_2 levels and the NO_3^- reservoir began to rise again, as recorded in the ~2.46 Ga Joffre Member and the ~2.45 Ga Weeli Wolli Iron Formation, marking a shift towards a more stable and well-oxygenated offshore seawater environment. Our study unveils a nonlinear process of redox evolution in the Archaean seawater, characterized by a substantial O_2 oscillation over hundreds of millions of years. If the GOE is marked by the Weeli Wolli Formation in the Hamersley Basin[45], our data suggest that a full oxygenation of offshore seawater occurred at least 5 million years earlier than the GOE.

Online content

Any methods, additional references, Nature Portfolio reporting summaries, source data, extended data, supplementary information, acknowledgements, peer review information; details of author contributions and competing interests; and statements of data and code availability are available at https://doi.org/10.1038/s41561-025-01683-7.

References

1. Lyons, T. W., Reinhard, C. T. & Planavsky, N. J. The rise of oxygen in Earth's early ocean and atmosphere. *Nature* **506**, 307–315 (2014).
2. Garvin, J., Buick, R., Anbar, A. D., Arnold, G. L. & Kaufman, A. J. Isotopic evidence for an aerobic nitrogen cycle in the latest Archean. *Science* **323**, 1045–1048 (2009).
3. Ostrander, C. M. et al. Fully oxygenated water columns over continental shelves before the Great Oxidation Event. *Nat. Geosci.* **12**, 186–191 (2019).
4. Kendall, B. et al. Pervasive oxygenation along late Archaean ocean margins. *Nat. Geosci.* **3**, 647–652 (2010).
5. Wang, C. et al. A craton-wide geochemical survey of late Archean banded iron formations in China. *Earth Planet. Sci. Lett.* **642**, 118879 (2024).
6. Stüeken, E. E., Catling, D. C. & Buick, R. Contributions to late Archaean sulphur cycling by life on land. *Nat. Geosci.* **5**, 722–725 (2012).
7. Planavsky, N. J. et al. Evidence for oxygenic photosynthesis half a billion years before the Great Oxidation Event. *Nat. Geosci.* **7**, 283–286 (2014).
8. Rosing, M. T. & Frei, R. U-rich Archaean sea-floor sediments from Greenland—indications of >3700 Ma oxygenic photosynthesis. *Earth Planet. Sci. Lett.* **217**, 237–244 (2004).
9. Anbar, A. D. et al. A whiff of oxygen before the great oxidation event? *Science* **317**, 1903–1906 (2007).
10. Lalonde, S. V. & Konhauser, K. O. Benthic perspective on Earth's oldest evidence for oxygenic photosynthesis. *Proc. Natl Acad. Sci. USA* **112**, 995–1000 (2015).
11. He, H. et al. An abiotic source of Archean hydrogen peroxide and oxygen that pre-dates oxygenic photosynthesis. *Nat. Commun.* **12**, 6611 (2021).
12. Busigny, V. & Bebout, G. E. Nitrogen in the silicate Earth: speciation and isotopic behavior during mineral-fluid interactions. *Elements* **9**, 353–358 (2013).
13. Stüeken, E. E., Kipp, M. A., Koehler, M. C. & Buick, R. The evolution of Earth's biogeochemical nitrogen cycle. *Earth Sci. Rev.* **160**, 220–239 (2016).
14. Zhang, X., Sigman, D. M., Morel, F. M. & Kraepiel, A. M. Nitrogen isotope fractionation by alternative nitrogenases and past ocean anoxia. *Proc. Natl Acad. Sci. USA* **111**, 4782–4787 (2014).
15. Zerkle, A. L., Junium, C. K., Canfield, D. E. & House, C. H. Production of ^{15}N-depleted biomass during cyanobacterial N_2-fixation at high Fe concentrations. *J. Geophys. Res. Biogeosci.* https://doi.org/10.1029/2007JG000651 (2008).

16. Casciotti, K. L. Inverse kinetic isotope fractionation during bacterial nitrite oxidation. *Geochim. Cosmochim. Acta* **73**, 2061–2076 (2009).
17. Thunell, R. C., Sigman, D. M., Muller-Karger, F., Astor, Y. & Varela, R. Nitrogen isotope dynamics of the Cariaco Basin, Venezuela. *Glob. Biogeochem. Cycles* https://doi.org/10.1029/2003GB002185 (2004).
18. Brunner, B. et al. Nitrogen isotope effects induced by anammox bacteria. *Proc. Natl Acad. Sci. USA* **110**, 18994–18999 (2013).
19. McCready, R. G. L., Gould, W. D. & Barendregt, R. W. Nitrogen isotope fractionation during the reduction of NO_3^- to NH_4^+ by *Desulfovibrio* sp. *Can. J. Microbiol.* **29**, 231–234 (1983).
20. Godfrey, L. V. & Falkowski, P. G. The cycling and redox state of nitrogen in the Archaean ocean. *Nat. Geosci.* **2**, 725–729 (2009).
21. Koehler, M. C., Buick, R., Kipp, M. A., Stueken, E. E. & Zaloumis, J. Transient surface ocean oxygenation recorded in the approximately 2.66 Ga Jeerinah Formation, Australia. *Proc. Natl Acad. Sci. USA* **115**, 7711–7716 (2018).
22. Busigny, V., Lebeau, O., Ader, M., Krapež, B. & Bekker, A. Nitrogen cycle in the late Archean ferruginous ocean. *Chem. Geol.* **362**, 115–130 (2013).
23. Luo, G. et al. Nitrogen fixation sustained productivity in the wake of the Palaeoproterozoic Great Oxygenation Event. *Nat. Commun.* **9**, 978 (2018).
24. Kipp, M. A., Stüeken, E. E., Yun, M., Bekker, A. & Buick, R. Pervasive aerobic nitrogen cycling in the surface ocean across the Paleoproterozoic Era. *Earth Planet. Sci. Lett.* **500**, 117–126 (2018).
25. Cheng, C. et al. Nitrogen isotope evidence for stepwise oxygenation of the ocean during the Great Oxidation Event. *Geochim. Cosmochim. Acta* **261**, 224–247 (2019).
26. Yamaguchi, K. *Geochemistry of Archean–Paleoproterozoic Black Shales: The Early Evolution of the Atmosphere, Oceans, and Biosphere*. Pennsylvania State University, PhD dissertation (2002).
27. Lantink, M. L., Davies, J., Ovtcharova, M. & Hilgen, F. J. Milankovitch cycles in banded iron formations constrain the Earth–Moon system 2.46 billion years ago. *Proc. Natl Acad. Sci. USA* **119**, e2117146119 (2022).
28. Lantink, M. L. et al. Towards an astrochronological framework for the lower Paleoproterozoic Kuruman and Brockman Iron formations. *S. Afr. J. Geol.* **127**, 325–358 (2024).
29. Poulton, S. W. et al. A 200-million-year delay in permanent atmospheric oxygenation. *Nature* **592**, 232–236 (2021).
30. Thomazo, C., Couradeau, E. & Garcia-Pichel, F. Possible nitrogen fertilization of the early Earth Ocean by microbial continental ecosystems. *Nat. Commun.* **9**, 2530 (2018).
31. Klein, C. & Beukes, N. J. Geochemistry and sedimentology of a facies transition from limestone to iron-formation deposition in the early Proterozoic Transvaal Supergroup, South Africa. *Econ. Geol.* **84**, 1733–1774 (1989).
32. Bekker, A. et al. Iron formation: the sedimentary product of a complex interplay among mantle, tectonic, oceanic, and biospheric processes. *Econ. Geol.* **105**, 467–508 (2010).
33. Konhauser, K. O. et al. Iron formations: a global record of Neoarchaean to Palaeoproterozoic environmental history. *Earth Sci. Rev.* **172**, 140–177 (2017).
34. Konhauser, K. O., Newman, D. K. & Kappler, A. The potential significance of microbial Fe(III) reduction during deposition of Precambrian banded iron formations. *Geobiology* **3**, 167–177 (2005).
35. Li, Y., Li, L. & Wu, Z. First-principles calculations of equilibrium nitrogen isotope fractionations among aqueous ammonium, silicate minerals and salts. *Geochim. Cosmochim. Acta* **297**, 220–232 (2021).
36. Bebout, G. E. & Fogel, M. L. Nitrogen-isotope compositions of metasedimentary rocks in the Catalina Schist, California: implications for metamorphic devolatilization history. *Geochim. Cosmochim. Acta* **56**, 2839–2849 (1992).
37. Hayes, J. in *Early Life on Earth* (ed. Bengston, S.) 220–236 (Columbia Univ. Press, 1994).
38. Boetius, A. et al. A marine microbial consortium apparently mediating anaerobic oxidation of methane. *Nature* **407**, 623–626 (2000).
39. Beal, E. J., House, C. H. & Orphan, V. J. Manganese- and iron-dependent marine methane oxidation. *Science* **325**, 184–187 (2009).
40. Haroon, M. F. et al. Anaerobic oxidation of methane coupled to nitrate reduction in a novel archaeal lineage. *Nature* **500**, 567–570 (2013).
41. Konhauser, K. O. et al. Decoupling photochemical Fe(II) oxidation from shallow-water BIF deposition. *Earth Planet. Sci. Lett.* **258**, 87–100 (2007).
42. Pellerin, A. et al. Iron-mediated anaerobic ammonium oxidation recorded in the early Archean ferruginous ocean. *Geobiology* **21**, 277–289 (2023).
43. Partridge, M. A., Golding, S. D., Baublys, K. A. & Young, E. Pyrite paragenesis and multiple sulfur isotope distribution in late Archean and early Paleoproterozoic Hamersley Basin sediments. *Earth Planet. Sci. Lett.* **272**, 41–49 (2008).
44. Li, Y. et al. Nitrogen isotopes as a robust tracer of fluid activities and mineral reactions in regional metamorphism. *Geochim. Cosmochim. Acta* **375**, 76–89 (2024).
45. Konhauser, K. O. et al. Aerobic bacterial pyrite oxidation and acid rock drainage during the Great Oxidation Event. *Nature* **478**, 369–373 (2011).
46. Lantink, M. L. et al. Precessional pacing of early Proterozoic redox cycles. *Earth Planet. Sci. Lett.* **610**, 118117 (2023).
47. Philippot, P. et al. Globally asynchronous sulphur isotope signals require re-definition of the Great Oxidation Event. *Nat. Commun.* **9**, 2245 (2018).
48. Eigenbrode, J. L. & Freeman, K. H. Late Archean rise of aerobic microbial ecosystems. *Proc. Natl Acad. Sci. USA* **103**, 15759–15764 (2006).
49. Gregory, D. D. et al. The chemical conditions of the late Archean Hamersley basin inferred from whole rock and pyrite geochemistry with $\Delta^{33}S$ and $\delta^{34}S$ isotope analyses. *Geochim. Cosmochim. Acta* **149**, 223–250 (2015).

Methods

Sample preparation

A total of 35 BIF core sections were selected (Extended Data Table 1), including 5 from the Marra Mamba Iron Formation, 8 from the Dale Gorge Member, 16 from the Joffre Member and 6 from the Weeli Wolli Formation. These core sections, each ~30 cm long originally, were provided by the Perth Core Library and the Rio Tinto Core Library in Perth, Western Australia. These samples were from four drill cores: DD98WRL1 (the Marra Mamba Formation, 154.3 m long, from depths of 524.6–678.9 m), DGM1 (the Dales Gorge Member, 142.11 m long, from depths of 0–142.11 m), DD98SGP001 (the Joffre Member, 283 m long, from depths of 89–372 m) and WW1 (the Weeli Wolli Formation, 272.2 m long, from depths of 0–272.2 m). For this study, a ~2 cm × 2 cm slab was cut from the iron-rich part of each core section (Extended Data Fig. 3), which was cleaned by removing surface material and subsequently crushed and ground to fine powder (<200 mesh) by hand using an agate mortar and pestle.

Major element analysis

The powdered samples were dissolved through a process involving HNO_3–H_2O_2–HF acids, with addition of H_3BO_4 to ensure complete dissolution of certain elements (for example, Si and Al; ref. 50). The solutions were analysed for major elements by inductively coupled plasma mass spectrometry on an Agilent 8800 at the Environmental Geochemistry Laboratory of the Department of Earth and Atmospheric Sciences, University of Alberta. The analysis gave a recovery ratio of >95% and a relative standard deviation of <5%, on the basis of the analysis of reference material GSR-1.

N isotope analysis

Nitrogen concentrations and isotope compositions of the BIFs were analysed using the offline sealed-tube combustion and extraction methods coupled with continuous-flow isotope ratio mass spectrometry[51]. In detail, the powdered samples were loaded in one-end-sealed quartz tubes with reagent Cu_xO_x and protection quartz wool. These tubes were loaded onto a custom-made metal manifold, evacuated overnight, sealed under high vacuum and then combusted at 900 °C for 8 h and 600 °C for 2 h to extract nitrogen in BIF into N_2. After combustion, the tubes were loaded back to the metal manifold and cracked under high vacuum. The released N_2 was cryogenically purified, quantified using a capacitance manometer and carried by ultrahigh-purity helium gas to a Thermo Finnegan MAT 253 mass spectrometer for N isotopic analysis[51]. All N isotope data were reported in the δ notation, where $\delta^{15}N_{sample} = (^{15}N/^{14}N)_{sample}/(^{15}N/^{14}N)_{standard} - 1$, with the standard being atmospheric N_2. On the basis of repeated analyses of samples and internal standard material that were calibrated by two certified reference materials (a low-organic content soil standard with N = 0.133 wt%, $\delta^{15}N = +6.97‰$ and a high-organic-content sediment standard with N = 0.52 wt%, $\delta^{15}N = +4.32‰$), the analytical error was <6% (2σ) for N concentration and <0.2‰ (2σ) for $\delta^{15}N$ values.

Rayleigh fractionation model

To determine whether the N isotopic signature of BIFs was significantly influenced by metamorphic N devolatilization, we modelled the N isotopic data using a simplified Rayleigh fractionation model:

$$\delta^{15}N_f = \delta^{15}N_i + 1000 \times \left(F^{(\alpha-1)} - 1\right) \qquad (1)$$

In this equation, $\delta^{15}N_i$ and $\delta^{15}N_f$ are the initial and final N isotope compositions of rocks, respectively; F represents the fraction of remaining N (which is normalized to K content to eliminate the influence of heterogeneous distribution of K-bearing minerals). Samples with the highest N/K ratios were considered as the least affected ones and thus best represent the initial isotopic signature. α is the temperature-dependent isotope fractionation factor between degassed species (N_2 or NH_3) and bonded NH_4^+ in silicate minerals, which can be calculated on the basis of parameters provided by refs. 35,52. A temperature (T) range of 250–400 °C was used to bracket the range of the prehnite–pumpellyite facies and greenschist facies. Since clay is the dominant N-bearing mineral, the α values for NH_3–bulk rock and N_2–bulk rock were approximately equal to those for NH_3–clay and N_2–clay. At $T = 250$ °C, the α values for NH_3–clay and N_2–clay are 0.9853 and 0.9925, respectively. At $T = 400$ °C, the α values for NH_3–clay and N_2–clay are 0.9901 and 0.9949. The modelling results indicate that the Hamersley BIF data do not follow the curves defined by metamorphic N devolatilization.

Box model

We used a box model to quantify the degree of denitrification (Fig. 2 and Extended Data Fig. 6). In this model, nitrogen fixation is the primary input to the ocean system, with water-column denitrification serving as the major output fluxes. For the seawater nitrate reservoir, the dominant input (>99%) is from nitrification, and the outputs are water-column denitrification and the burial of biomass from nitrate-assimilating organisms. Since water-column denitrification is ~80 times faster than sedimentary denitrification, and expansion of denitrification in the open ocean waters would lead to faster nitrate loss from the ocean[24], sedimentary denitrification is not treated separately in the model.

The isotopic composition of $N_{assimilators}$ can be determined using an open-system Rayleigh model:

$$\delta^{15}N_{\text{assimilator\_burial}} = \delta^{15}N_{\text{input}} + \left(\varepsilon \times \ln\left(1 - f_{\text{water-column-denitrification}}\right)\right) \qquad (2)$$

where $f_{\text{water-column-denitrification}}$ denotes the fraction of the nitrate reservoir removed by denitrification in the water column, and it was set between 0 and 1. The $\delta^{15}N_{input}$ was set at 0‰. The isotopic enrichment factor (ε) of water-column denitrification was assigned a range of −30‰ to −22‰, with an average value of −26‰ (ref. 53).

The total export production (total burial) can be described as:

$$f_{\text{total\_burial}} = f_{\text{assimilator\_burial}} + f_{\text{fixer\_burial}} \qquad (3)$$

where $f_{\text{fixer\_burial}}$ represents the fraction of nitrogen in N_2-fixing organisms that avoids re-mineralization in the water column and pore waters, and $f_{\text{assimilator\_burial}}$ represents the fraction of burial of nitrate-assimilating biomass.

If the marine N cycle is assumed to be at a steady state where N is not the limiting nutrient[54], an increase in denitrification would reduce export production from nitrate-assimilating organisms, resulting in a greater proportion of export production coming from N-fixing organisms. However, a decrease in the seawater O_2 level (an increase in the degree of denitrification) could be associated with trace metal limitation[55,56], which would in turn affect the total N fixation flux and thus lead to lower total N burial. To better fit our data, we determined:

$$f_{\text{total\_burial\_final}} = 1 \qquad (4)$$

$$f_{\text{total\_burial\_initial}} = 0.5 \qquad (5)$$

The $f_{\text{total\_burial}}$ decreases incrementally as the degree of denitrification increases. At the beginning of denitrification, $f_{\text{assimilator\_burial}}$ equals 1, and $f_{\text{fixer\_burial}}$ equals 0. At the final stage, $f_{\text{assimilator\_burial}}$ equals 0, and $f_{\text{fixer\_burial}}$ equals 0.5. This assumption is justified by post-depositional processes that are otherwise not accounted for in the model.

The nitrogen isotopic composition of marine sediments can be determined by:

$$\delta^{15}N_{\text{total\_burial}} = \frac{\left(\delta^{15}N_{\text{fixer\_burial}} \times f_{\text{fixer\_burial}}\right) + \left(\delta^{15}N_{\text{assimilator\_burial}} \times f_{\text{assimilator\_burial}}\right)}{f_{\text{fixer\_burial}} + f_{\text{assimilator\_burial}}} \qquad (6)$$

where $\delta^{15}N_{\text{fixer\_burial}}$ was assigned as 0‰ (ref. 15). The $f_{\text{water-column-denitrification}}$ in Fig. 2b was determined using a polynomial function that fits the solid black line in Fig. 2a.

The LOWESS curve

The secular trend for the nitrogen isotopic record in the Hamersley BIFs was generated using the LOWESS curve, which is a non-parametric smoothing algorithm designed to visualize trends in irregularly spaced time-series data through local fitting[57]. During the fitting, the d value was set at 1, which means that the local fits were performed via linear regression. The width of the moving window (f) was set at 0.3 to minimize variability in the smoothed points while preserving trends in the data[57]. All LOWESS calculations were conducted in the Python Environment using the statsmodels library.

Age constraints

Geochronological constraints on the Hamersley Group have been established by previous studies. Zircon sensitive high-resolution ion microprobe U–Pb ages were reported by several studies. Reference 58 reported an age of 2,470 ± 4 Ma for a tuff band in the Dales Gorge Member and an age of 2,449 ± 3 Ma for a felsic tuffaceous sandstone sample in the Weeli Wolli Formation. Reference 59 reported an age of 2,597 ± 5 Ma from a shale band in the Mt Newman Member of the Marra Mamba Formation. Reference 60 reported ages of 2,454 ± 3 Ma and 2,459 ± 3 Ma from siliceous tuffaceous mudstones in the Joffre Member. Reference 61 reported an age of 2,629 ± 5 Ma for a tuff band in the Roy Hill Shale Member of the Jeerinah Formation and an age of 2,463 ± 5 Ma for the Whaleback Shale Member. Reference 62 reported an age of 2,684 ± 6 Ma for the Nallanaring Volcanic Member of the Jeerinah Formation. Reference 9 reported a Re–Os age of 2,501.1 ± 8.2 Ma for the Mt McRae Shale Formation. More recently, refs. 27,28,46 carried out high-precision U-Pb zircon dating by chemical abrasion, isotope dilution, thermal ionization mass spectrometry, which gave ages of 2,454.0 ± 0.6 Ma, 2,459 ± 1.3 Ma, 2,462.9 ± 1.34 Ma and 2,469.1 ± 0.65 Ma for shale horizons within the Joffre Member, as well as ages of 2,482.1 ± 1.9 Ma and 2,477.8 ± 0.94 Ma for the S1 and S9 shale horizons in the Dales Gorge Member.

Data availability

All data supporting this study are provided in Extended Data Table 1 and are available via figshare at https://doi.org/10.6084/m9.figshare.26094001 (ref. 63). Source data are provided with this paper.

References

50. Wu, S., Zhao, Y.-H., Feng, X. & Wittmeier, A. Application of inductively coupled plasma mass spectrometry for total metal determination in silicon-containing solid samples using the microwave-assisted nitric acid–hydrofluoric acid–hydrogen peroxide–boric acid digestion system. *J. Anal. At. Spectrom.* **11**, 287–296 (1996).
51. Li, L. et al. Recommendations for offline combustion-based nitrogen isotopic analysis of silicate minerals and rocks. *Rapid Commun. Mass Spectrom.* **35**, e9075 (2021).
52. Li, L., He, Y., Zhang, Z. & Liu, Y. Nitrogen isotope fractionations among gaseous and aqueous NH_4^+, NH_3, N_2, and metal-ammine complexes: theoretical calculations and applications. *Geochim. Cosmochim. Acta* **295**, 80–97 (2021).
53. Devol, A. H. Denitrification, anammox, and N_2 production in marine sediments. *Ann. Rev. Mar. Sci.* **7**, 403–423 (2015).
54. Tyrrell, T. The relative influences of nitrogen and phosphorus on oceanic primary production. *Nature* **400**, 525–531 (1999).
55. Jones, C., Nomosatryo, S., Crowe, S. A., Bjerrum, C. J. & Canfield, D. E. Iron oxides, divalent cations, silica, and the early Earth phosphorus crisis. *Geology* **43**, 135–138 (2015).
56. Anbar, A. D. & Knoll, A. H. Proterozoic ocean chemistry and evolution: a bioinorganic bridge? *Science* **297**, 1137–1142 (2002).
57. Cleveland, W. S. Robust locally weighted regression and smoothing scatterplots. *J. Am. Stat. Assoc.* **74**, 829–836 (1979).
58. Barley, M. E., Pickard, A. L. & Sylvester, P. J. Emplacement of a large igneous province as a possible cause of banded iron formation 2.45 billion years ago. *Nature* **385**, 55–58 (1997).
59. Trendall, A. F., Nelson, D. R., De Laeter, J. R. & Hassler, S. W. Precise zircon U–Pb ages from the Marra Mamba Iron Formation and Wittenoom Formation, Hamersley Group, Western Australia. *Aust. J. Earth Sci.* **45**, 137–142 (1998).
60. Pickard, A. L. SHRIMP U–Pb zircon ages of tuffaceous mudrocks in the Brockman Iron Formation of the Hamersley Range, Western Australia. *Aust. J. Earth Sci.* **49**, 491–507 (2002).
61. Trendall, A. F., Compston, W., Nelson, D. R., De Laeter, J. R. & Bennett, V. C. SHRIMP zircon ages constraining the depositional chronology of the Hamersley Group, Western Australia. *Aust. J. Earth Sci.* **51**, 621–644 (2004).
62. Arndt, N. T., Nelson, D. R., Compston, W., Trendall, A. F. & Thorne, A. M. The age of the Fortescue Group, Hamersley Basin, Western Australia, from ion microprobe zircon U–Pb results. *Aust. J. Earth Sci.* **38**, 261–281 (2007).
63. Liang, X., Stüeken, E. E., Alessi, D. S., Konhauser, K. O. & Li, L. Data for 'A seawater oxygen oscillation recorded by iron formations prior to the Great Oxidation Event'. *Figshare* https://doi.org/10.6084/m9.figshare.26094001 (2025).
64. Rasmussen, B. & Muhling, J. R. Development of a greenalite–silica shuttle during incursions of hydrothermal vent plumes onto Neoarchean shelf, Hamersley region, Australia. *Precambrian Res.* **353**, 106003 (2021).

Acknowledgements

This work was supported by the National Sciences and Engineering Research Council of Canada (NSERC) under grant no. RGPIN-2019-06003 (for L.L.) and RGPIN-165831 (for K.O.K.). E.E.S. acknowledges funding from a NERC Frontiers grant (NE/V010824/1). Samples used in this study were made available by the Geological Survey of Western Australia (GSWA). We thank GSWA for the drill core information. K.O.K. also acknowledges support from the Royal Society and the Wolfson Foundation, provided through the Royal Society Wolfson Visiting Fellowship.

Author contributions

X.L., L.L. and K.O.K. conceptualized the study. X.L. performed the N isotopic analyses, major elements analyses and visualization. L.L., K.O.K., E.E.S. and D.S.A. contributed to the methodology of modelling and analyses. X.L., L.L., K.O.K. and E.E.S. prepared the manuscript. All co-authors reviewed and commented on the manuscript.

Competing interests

The authors declare no competing interests.

Additional information

Extended data is available for this paper at https://doi.org/10.1038/s41561-025-01683-7.

Supplementary information The online version contains supplementary material available at https://doi.org/10.1038/s41561-025-01683-7.

Correspondence and requests for materials should be addressed to Xueqi Liang.

Peer review information *Nature Geoscience* thanks Vincent Busigny and Margriet L. Lantink for their contribution to the peer review of this work. Primary Handling Editor: Alison Hunt, in collaboration with the *Nature Geoscience* team.

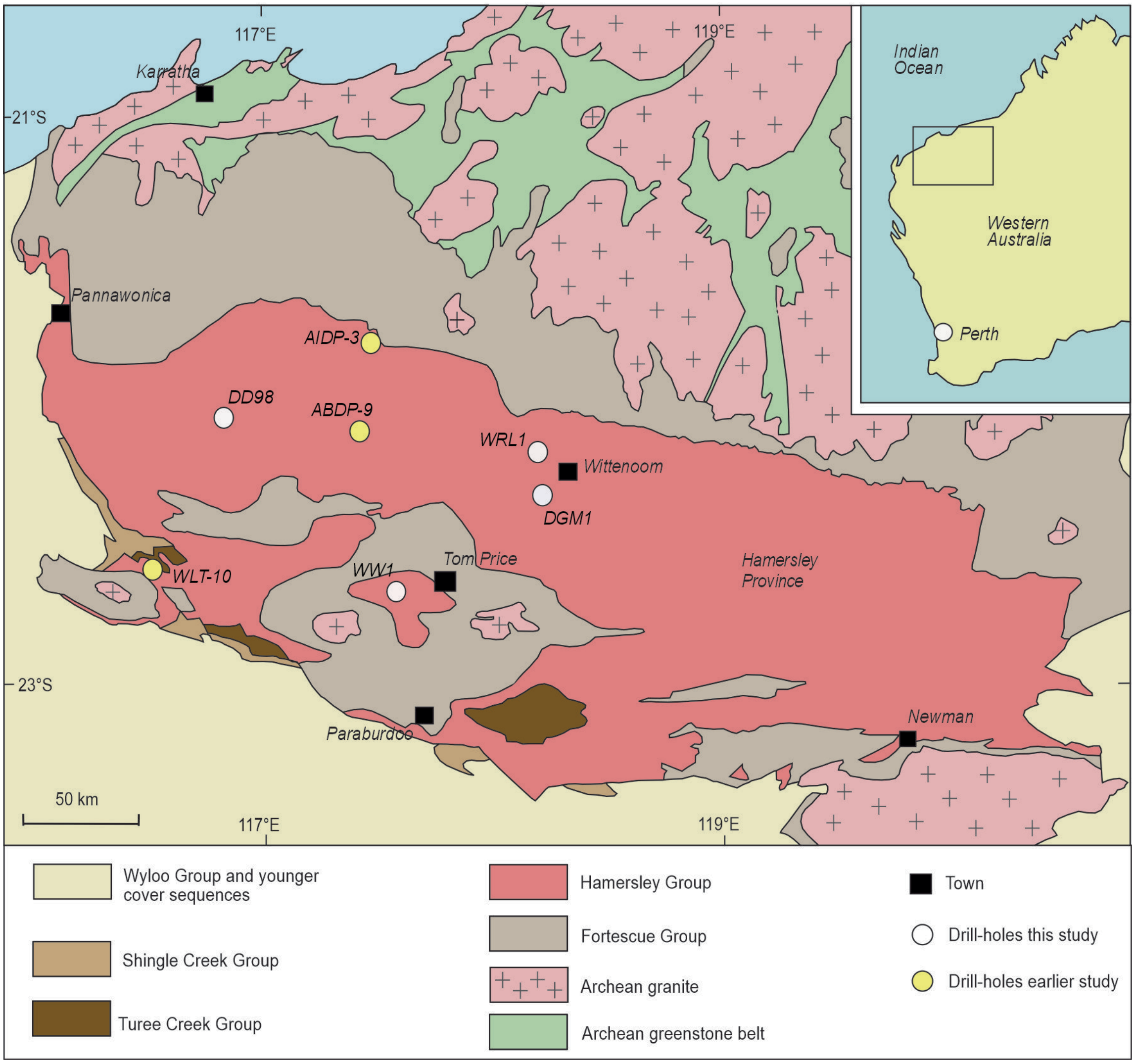

Extended Data Fig. 1 | Geological map of the Hamersley Province, northwestern Australia, showing the location of the sampled drill holes. Figure reproduced with permission from ref. 64, Elsevier.

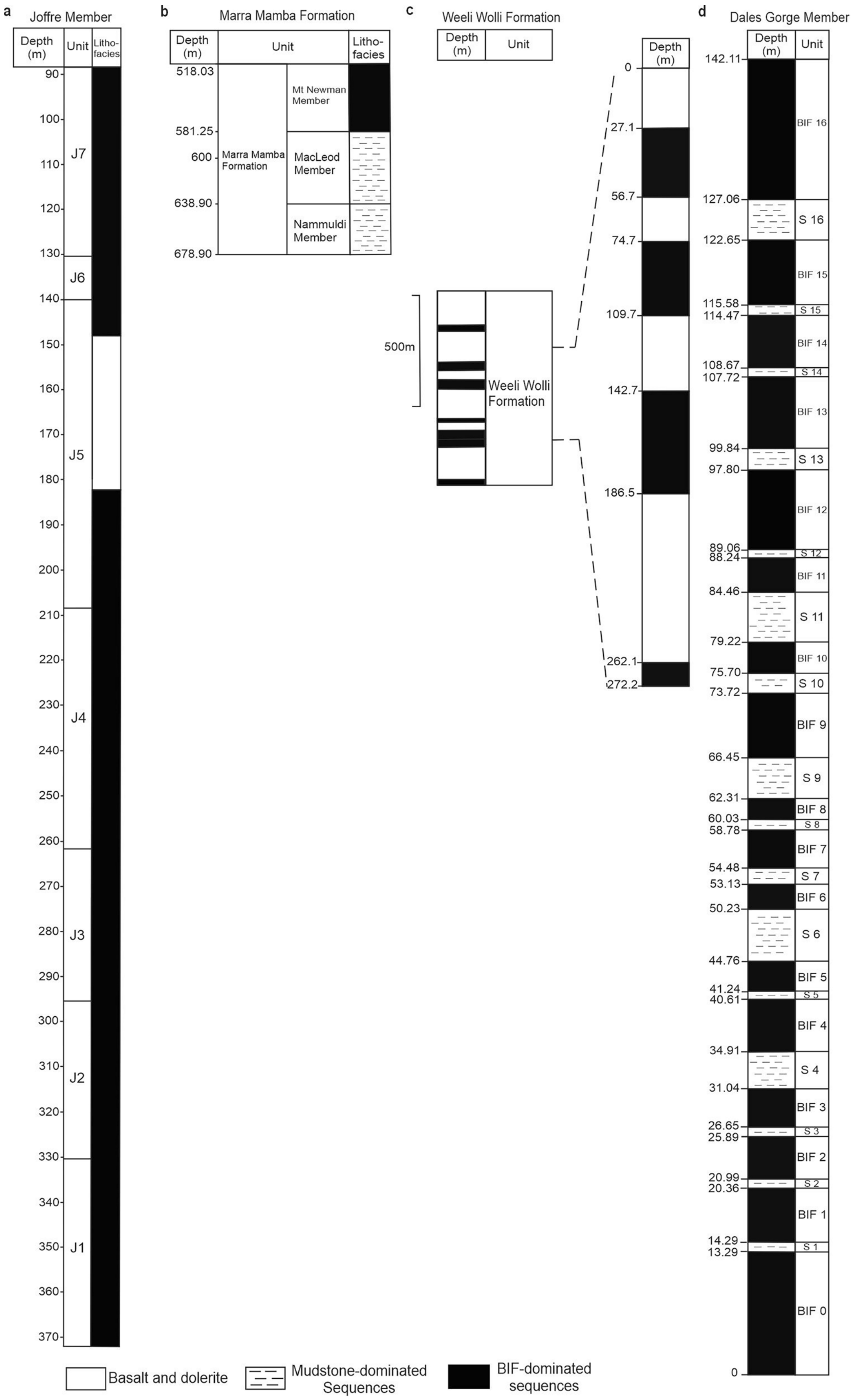

Extended Data Fig. 2 | Stratigraphic column of drill cores DD98, WRL1, WW1 and DGM1. Drill core data of (a) Joffre Member, (b) Marra Mamba Formation, (c) Weeli Wolli Formation and (d) Dales Gorge Member are from the Geological Survey of Western Australia.

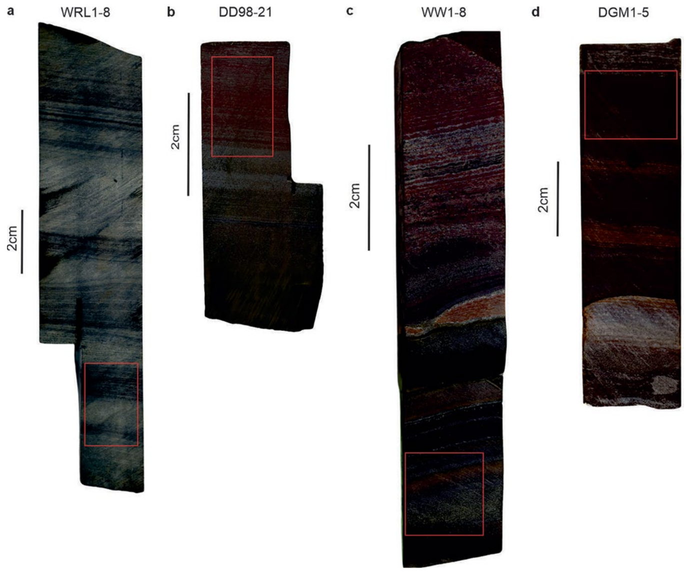

Extended Data Fig. 3 | Core photos of representative BIF samples. Red boxes represent the sampling locations of samples (a) WRL 1-8, (b) DD98-21, (c) WW1-8 and (d) DGM1-5.

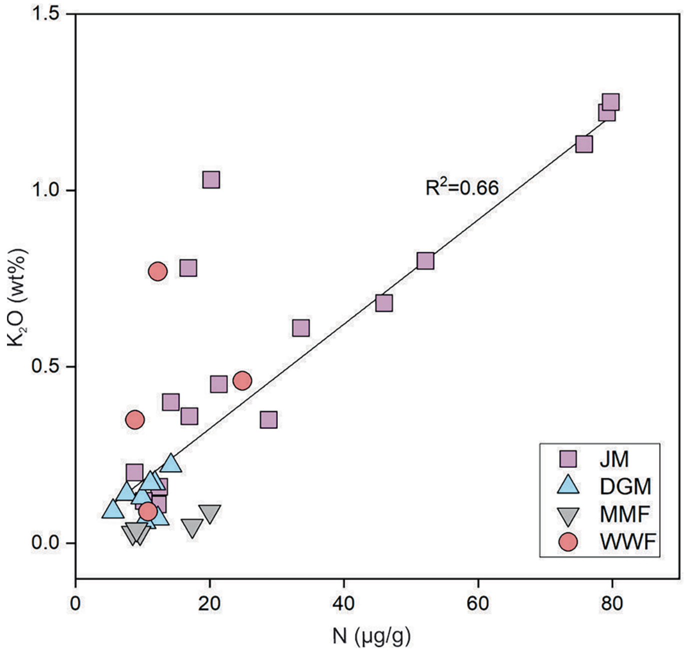

Extended Data Fig. 4 | Comparison of N concentrations with K_2O concentrations of the studied BIF samples. Note that the two samples with exceptional high Al_2O_3 contents (>2 wt.%) are not included. 2σ error bars of the data are smaller than the symbols and thus not shown. WWF = Weeli Wolli Formation; JM = Joffre Member; DGM = Dales Gorge Member; MMF = Marra Mamba Formation.

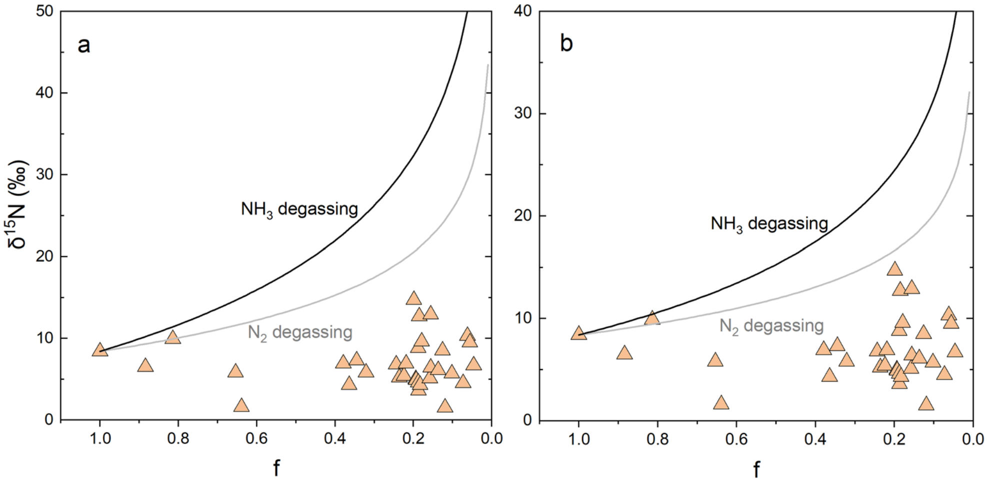

Extended Data Fig. 5 | Comparison of the $\delta^{15}N$ values of BIFs (triangles) and theoretical curves of metamorphic N devolatilization calculated by Rayleigh fractionation modeling. Temperature is set at 250 °C for Panel (**a**) and 400 °C for panel (**b**) (see Methods). 2σ error bars of the data are smaller than the symbols and thus not shown.

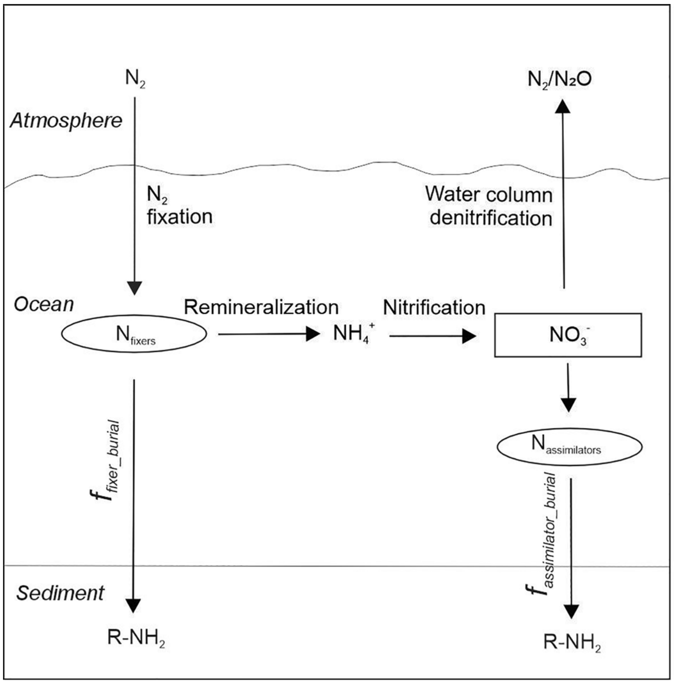

Extended Data Fig. 6 | Schematic box model of the nitrogen cycle on Earth's surface. See 'Box model' section in the Methods for details.

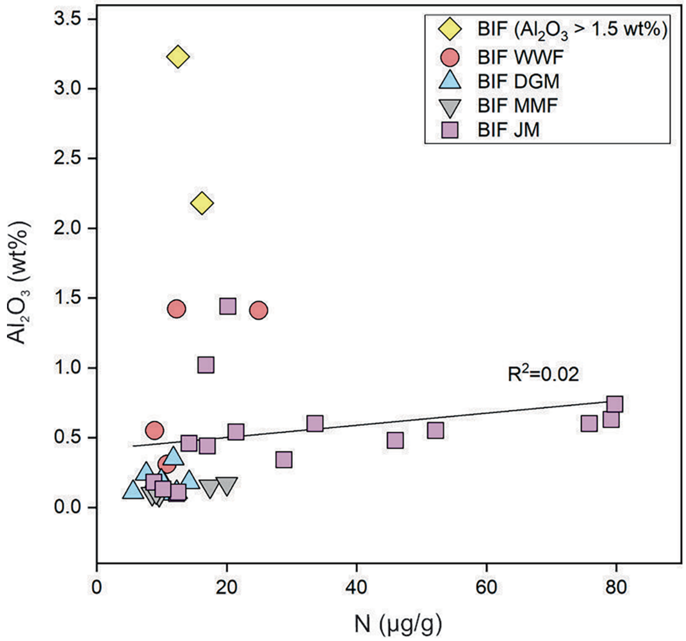

Extended Data Fig. 7 | Comparison of N concentrations with Al_2O_3 concentrations of the studied BIF samples. 2σ error bars of the data are smaller than the symbols and thus not shown. WWF = Weeli Wolli Formation; JM = Joffre Member; DGM = Dales Gorge Member; MMF = Marra Mamba Formation.

Extended Data Table 1 | Geochemical data for Hamersley BIFs

Sample ID	Depth (m)	$\delta^{15}N$ (‰)	N (µg/g)	Al_2O_3 (wt.%)	K_2O (wt.%)
Weeli Wolli Formation					
WW1-3	51.2	7.3	10.8	0.31	0.09
WW1-6	80.7	4.5	8.9	0.55	0.35
WW1-8	94.8	1.5	16.2	2.18	0.39
WW1-13	148.1	6.4	24.9	1.41	0.46
WW1-18	180.9	3.7	12.5	3.23	0.77
WW1-19	267.3	6.7	12.3	1.42	0.77
Joffre Member					
DD98-1	94.0	4.6	52.2	0.55	0.80
DD98-2	100.7	3.6	79.2	0.63	1.22
DD98-3	110.5	5.8	12.3	0.10	0.11
DD98-4	120.3	5.2	28.8	0.34	0.35
DD98-7	146.6	9.2	17.0	0.44	0.36
DD98-8	161.9	4.3	79.8	0.74	1.25
DD98-9	191.3	6.1	21.4	0.54	0.45
DD98-10	197.0	5.7	14.2	0.46	0.40
DD98-15A	209.3	5.4	12.5	0.11	0.16
DD98-16	232.8	4.9	75.8	0.60	1.13
DD98-19B	251.7	5.0	46.0	0.48	0.68
DD98-21	281.6	5.1	33.6	0.60	0.61
DD98-22	300.2	8.5	8.8	0.18	0.20
DD98-23	310.4	6.8	10.2	0.13	0.12
DD98-24	358.2	10.3	16.8	1.02	0.78
DD98-25	364.3	9.5	20.2	1.44	1.03
Dales Gorge Member					
DGM1-1	8.5	12.9	7.6	0.24	0.14
DGM1-2	27.1	7.2	12.3	0.11	0.07
DGM1-4	42.7	11.6	10.3	0.17	0.06
DGM1-5	60.4	14.7	11.8	0.35	0.17
DGM1-6	77.1	6.9	9.9	0.19	0.13
DGM1-7	91.7	8.8	11.1	0.10	0.17
DGM1-8	110.3	9.6	5.6	0.11	0.09
DGM 1-16	139.0	12.7	14.2	0.18	0.22
Marra Mamba Formation					
WRL1-2	532.0	9.9	8.5	0.10	0.03
WRL1-5	563.3	8.4	17.4	0.15	0.05
WRL1-6	572.6	8.4	9.6	0.09	0.03
WRL1-8	589.5	1.6	20.0	0.17	0.09
WRL1-9	593.3	5.8	9.1	0.11	0.04